JACS
JOURNAL OF THE AMERICAN CHEMICAL SOCIETY

Subscriber access provided by ISTANBUL TEKNIK UNIV

Article

A Microfluidic Fuel Cell with Flow-Through Porous Electrodes

Erik Kjeang, Raphaelle Michel, David A. Harrington, Ned Djilali, and David Sinton

J. Am. Chem. Soc., **2008**, 130 (12), 4000-4006 • DOI: 10.1021/ja078248c

Downloaded from http://pubs.acs.org on February 8, 2009

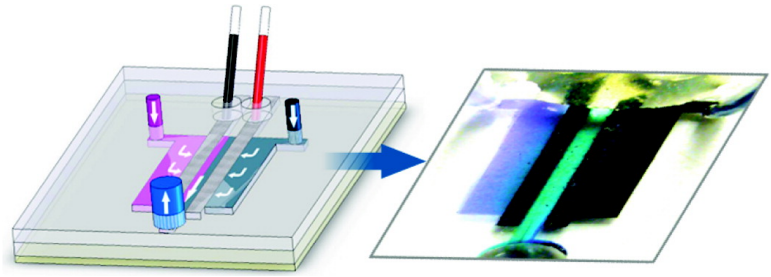

More About This Article

Additional resources and features associated with this article are available within the HTML version:

- Supporting Information
- Links to the 1 articles that cite this article, as of the time of this article download
- Access to high resolution figures
- Links to articles and content related to this article
- Copyright permission to reproduce figures and/or text from this article

View the Full Text HTML

ACS Publications
High quality. High impact.

Journal of the American Chemical Society is published by the American Chemical Society. 1155 Sixteenth Street N.W., Washington, DC 20036

J|A|C|S
ARTICLES
Published on Web 03/04/2008

A Microfluidic Fuel Cell with Flow-Through Porous Electrodes

Erik Kjeang,[†] Raphaelle Michel,[†] David A. Harrington,[‡] Ned Djilali,[†] and David Sinton*[,†]

Department of Mechanical Engineering, Department of Chemistry, and Institute for Integrated Energy Systems (IESVic), University of Victoria, 3800 Finnerty Road, Victoria, BC, V8W2Y2, Canada

Received October 28, 2007; E-mail: dsinton@me.uvic.ca

Abstract: A microfluidic fuel cell architecture incorporating flow-through porous electrodes is demonstrated. The design is based on cross-flow of aqueous vanadium redox species through the electrodes into an orthogonally arranged co-laminar exit channel, where the waste solutions provide ionic charge transfer in a membraneless configuration. This flow-through architecture enables improved utilization of the three-dimensional active area inside the porous electrodes and provides enhanced rates of convective/diffusive transport without increasing the parasitic loss required to drive the flow. Prototype fuel cells are fabricated by rapid prototyping with total material cost estimated at 2 USD/unit. Improved performance as compared to previous microfluidic fuel cells is demonstrated, including power densities at room temperature up to 131 mW cm^{-2}. In addition, high overall energy conversion efficiency is obtained through a combination of relatively high levels of fuel utilization and cell voltage. When operated at 1 μL min^{-1} flow rate, the fuel cell produced 20 mW cm^{-2} at 0.8 V combined with an active fuel utilization of 94%. Finally, we demonstrate in situ fuel and oxidant regeneration by running the flow-through architecture fuel cell in reverse.

1. Introduction

The high-energy density demand in portable applications is making microstructured fuel cells an increasingly attractive technology.[1] Microfluidic fuel cells,[2−17] or laminar flow-based fuel cells, represent a relatively new type of small scale fuel cell technology based on inexpensive microfabrication methods and low-cost materials. A microfluidic fuel cell is defined as a device that incorporates all fundamental components of a fuel cell to a single microfluidic channel and its walls. Such fuel cells operate without a membrane, and the most common configurations rely on the laminar nature of microscale flows to maintain sufficient separation of fuel and oxidant streams. Ionic charge transfer is facilitated by a supporting electrolyte contained in the co-laminar streams. Interdiffusion is restricted to an interfacial width at the center of the channel, and the electrodes are positioned sufficiently far away from this interdiffusion zone to prevent crossover effects. Microfluidic fuel cells provide a number of unique advantages: fuel and oxidant streams may be combined in a single microchannel; no ion exchange membrane is needed; sealing, manifolding, and fluid delivery requirements are reduced; and issues related to membrane hydration and water management are eliminated.

Microfluidic fuel cell devices have been demonstrated based on a number of fuels, including vanadium ions,[9,14,15] formic acid,[4,8,12,13] methanol,[5,6,11] hydrogen,[7,16,17] and hydrogen peroxide,[10] combined with oxidants such as vanadium ions,[9,14,15] oxygen,[4−8,11,12,16,17] or hydrogen peroxide.[10,13] The power densities of these cells were mainly restricted by the solubility of the reactants and the associated rate of convective/diffusive mass transport to the active sites.[3] Cell designs using oxygen have the benefit of "free" oxidant available in the ambient air. Such air-breathing designs require a blank cathodic electrolyte stream and have shown moderate power densities. The highest power density levels of the microfluidic fuel cells reported to date were achieved using vanadium redox couples in both half cells: V^{2+}/V^{3+} as anolyte and VO^{2+}/VO_2^{+} as catholyte.[9,14,15] These vanadium redox fuel cells benefit from a rapid and balanced

[†] Department of Mechanical Engineering (IESVic).
[‡] Department of Chemistry and IESVic.

(1) Dyer, C. K. *J. Power Sources* **2002**, *106*, 31−34.
(2) Bazylak, A.; Sinton, D.; Djilali, N. *J. Power Sources* **2005**, *143*, 57−66.
(3) Chang, M. H.; Chen, F.; Fang, N. S. *J. Power Sources* **2006**, *159*, 810−816.
(4) Choban, E. R.; Markoski, L. J.; Wieckowski, A.; Kenis, P. J. A. *J. Power Sources* **2004**, *128*, 54−60.
(5) Choban, E. R.; Spendelow, J. S.; Gancs, L.; Wieckowski, A.; Kenis, P. J. A. *Electrochim. Acta* **2005**, *50*, 5390−5398.
(6) Choban, E. R.; Waszczuk, P.; Kenis, P. J. A. *Electrochem. Solid State Lett.* **2005**, *8*, A348−A352.
(7) Cohen, J. L.; Volpe, D. J.; Westly, D. A.; Pechenik, A.; Abruna, H. D. *Langmuir* **2005**, *21*, 3544−3550.
(8) Cohen, J. L.; Westly, D. A.; Pechenik, A.; Abruna, H. D. *J. Power Sources* **2005**, *139*, 96−105.
(9) Ferrigno, R.; Stroock, A. D.; Clark, T. D.; Mayer, M.; Whitesides, G. M. *J. Am. Chem. Soc.* **2002**, *124*, 12930−12931.
(10) Hasegawa, S.; Shimotani, K.; Kishi, K.; Watanabe, H. *Electrochem. Solid State Lett.* **2005**, *8*, A119−A121.
(11) Jayashree, R. S.; Egas, D.; Spendelow, J. S.; Natarajan, D.; Markoski, L. J.; Kenis, P. J. A. *Electrochem. Solid State Lett.* **2006**, *9*, A252−A256.
(12) Jayashree, R. S.; Gancs, L.; Choban, E. R.; Primak, A.; Natarajan, D.; Markoski, L. J.; Kenis, P. J. A. *J. Am. Chem. Soc.* **2005**, *127*, 16758−16759.
(13) Kjeang, E.; Brolo, A. G.; Harrington, D. A.; Djilali, N.; Sinton, D. *J. Electrochem. Soc.* **2007**, *154*, B1220−B1226.
(14) Kjeang, E.; McKechnie, J.; Sinton, D.; Djilali, N. *J. Power Sources* **2007**, *168*, 379−390.
(15) Kjeang, E.; Proctor, B. T.; Brolo, A. G.; Harrington, D. A.; Djilali, N.; Sinton, D. *Electrochim. Acta* **2007**, *52*, 4942−4946.
(16) Mitrovski, S. M.; Elliott, L. C. C.; Nuzzo, R. G. *Langmuir* **2004**, *20*, 6974−6976.
(17) Mitrovski, S. M.; Nuzzo, R. G. *Lab-on-a-Chip* **2006**, *6*, 353−361.

10.1021/ja078248c CCC: $40.75 **© 2008 American Chemical Society**

electrochemical system in terms of species transport characteristics and reaction rates, as well as a relatively high open-circuit voltage (~1.5 V). In addition, the vanadium redox reactions take place on carbon electrodes without any additional electrocatalyst and associated cost.

The capability of reaching high levels of fuel utilization per single pass has been a major challenge associated with microfluidic fuel cell technology to date.[2] In previous work,[14,15] we demonstrated that a high aspect ratio (width/height) cross-sectional channel geometry in combination with the all-liquid vanadium redox system enabled fuel utilization levels around 50% per single pass at low flow rates. Although improved over previous designs, fuel utilization was still limited by geometrical constraints, and high fuel utilization could only be achieved at low cell voltages. It was also demonstrated that incorporating porous electrodes[15] provided up to 72% higher power density than planar electrodes; an improvement attributed to the increased active area and the enhanced species transport characteristics resulting from some flow penetration within the porous medium. To reach practical energy conversion efficiency, however, it is necessary to sustain high levels of fuel utilization at high power densities and, perhaps more importantly, at high operational cell voltages.

Microfluidic fuel cells have additional characteristics that have yet to be exploited through fuel cell design. Specifically, the reactants, products, and electrolyte co-exist in the same liquid phase, and the reaction zones are solid−liquid interfaces. These characteristics provide potential for a variety of three-dimensional fuel cell architectures. In this work, we present a microfluidic fuel cell incorporating flow-through porous electrodes. The proposed microfluidic fuel cell has two unique features: (i) hydrophilic electrode treatment that promotes saturation of the porous electrode, and thus increases the effective active area; and (ii) a three-dimensional flow-through architecture that improves utilization of the active area through enhanced transport.

2. Methods

2.1. Microfabrication. Microfluidic fuel cell prototypes of the flow-through electrode architecture as well as the established architecture[15] with electrodes mounted on the bottom of a co-laminar flow channel were assembled using in-house developed microfabrication techniques. The previously established architecture will be termed "flow-over", to differentiate it from the "flow-through" architecture developed through this work. The fabrication procedures for the two designs differ somewhat and are presented separately in the following subsections.

2.1.1. Flow-Through Architecture Fuel Cell. Porous carbon strip electrodes were cut to size (20 mm long and 1 mm wide) from sheets of Toray carbon paper (B-2 Designation TGPH-090; E-TEK) with typical thickness 300 μm (measured), typical density 0.49 g cm^{-3}, and 78% porosity. This carbon paper is manufactured primarily for use in polymer electrolyte membrane fuel cells, and a PTFE coating is applied at the time of manufacture to achieve a hydrophobic surface condition as required for that application. For the purposes of this work, the hydrophobic coating on the carbon strips was depolymerized and removed by annealing (~1 s) in a propane flame. The heat-treated carbon strips were fitted in custom-sized grooves (20 mm × 1 mm × 300 μm, separated by 1 mm), fabricated by replica molding in poly(dimethylsiloxane) (PDMS; Dow Corning) according to established soft-lithographic protocols.[18] A 300 μm high master that defines the two

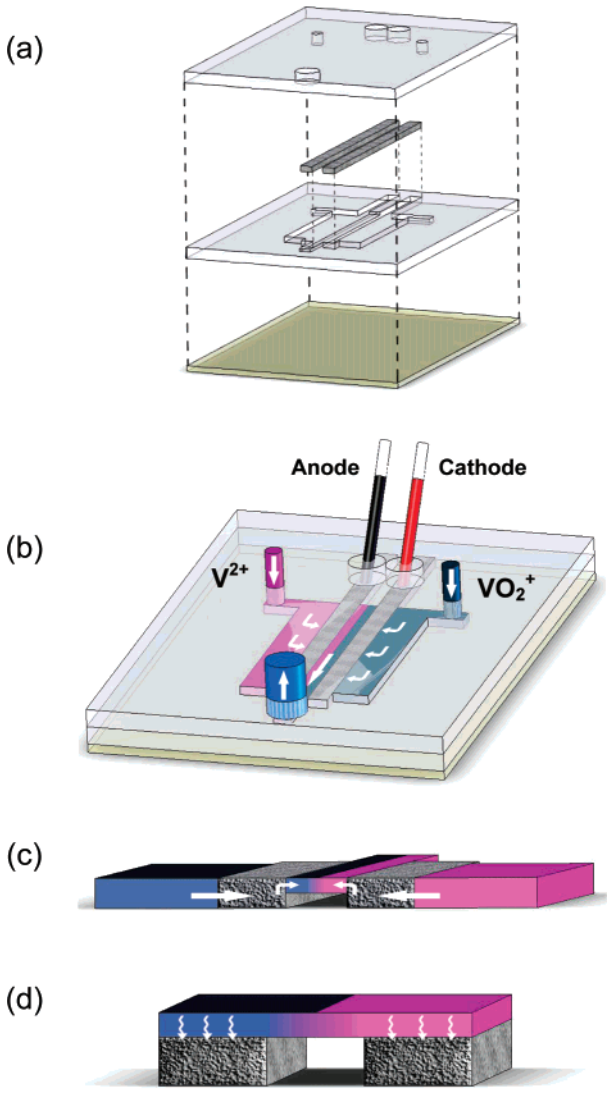

Figure 1. Schematics of (a) fabrication and (b) operation of the microfluidic fuel cell architecture with flow-through electrodes, and cross-sectional geometry of (c) the new flow-through architecture and (d) the established flow-over architecture fuel cell, employing aqueous vanadium redox species as fuel (V^{2+} - light purple - on right) and oxidant (VO_2^+ - blue/black - on left). The solution colors shown are characteristic of the employed solutions.

grooves and the channel structure was created by photolithography in negative photoresist (SU-8 50; Microchem). The master had a dual-layer structure. The first layer was 150 μm thick and encompassed all flow channels and electrode grooves. The second layer, which was also 150 μm thick and patterned on top of the first layer, included electrode grooves and the channel pattern from the inlets to the electrodes. Upon casting of this dual-layered master into PDMS, a negative imprint was obtained that accommodated both electrode grooves and complete fluid manifolding. As shown schematically in Figure 1a, the obtained PDMS part was placed face up on a 1″ × 3″ microscope glass slide for structural support, and the heat-treated carbon strip electrodes were fitted in its grooves, thereby finalizing the bottom part of the fuel cell. The top of the cell was sealed with a flat layer of PDMS, with previously punched holes for the inlets, outlet, and electrical contacts. An irreversible seal was created by plasma-treating both PDMS parts, which renders hydrophilic channel walls and facilitates covalent binding upon assembly. The holes in the top PDMS part were aligned with the grooves of the bottom part during assembly of the final device (Figure 1a). The electrodes of the assembled fuel cell had an active volume of 0.3 mm × 1 mm × 12 mm (3.6 μL). Wires were attached to the exposed ends of the carbon electrodes using PELCO conductive silver 187 (Ted

(18) Duffy, D. C.; McDonald, J. C.; Schueller, O. J. A.; Whitesides, G. M. *Anal. Chem.* **1998**, *70*, 4974−4984.

Pella, Inc.). The co-laminar flow of vanadium solutions through the fuel cell was driven by a syringe pump (PHD 2000; Harvard Apparatus) via Teflon tubing (1/16″ diameter; S.P.E. Limited) to the inlets and a larger Tygon tube (3 mm diameter; Fisher Scientific) from the outlet to the outlet reservoir. The described fabrication procedure is relatively quick and economical. Excluding external wires and tubes, the fuel cell contained only PDMS and carbon paper, and the total estimated material cost is 2 USD per cell. These fuel cells have an advantage with respect to cost as compared to conventional fuel cells that require precious metal catalysts.

2.1.2. Flow-Over Architecture Fuel Cell. Fuel cells with the established flow-over architecture[15] were fabricated according to the procedure outlined in section 2.1.1, with the following modifications. The flow-over unit consisted of two parts. A bottom PDMS part contained the electrodes and a top PDMS part accommodated the microfluidic channel network. The bottom part was a PDMS slab with two custom-shaped grooves (20 mm × 1 mm × 300 μm) separated by 1 mm. The carbon strip electrodes were fitted into these grooves. The top part contained a T-shaped 150 μm-high and 3 mm-wide microchannel that was aligned with the carbon electrodes during assembly.

2.2. Preparation of Vanadium Solutions. Vanadium stock electrolyte was purchased from Highveld and received as 2 M vanadium redox species (50/50 V^{3+}/VO^{2+}) in 4 M sulfuric acid with proprietary stabilizing agents. The V^{2+} and VO_2^+ solutions used as anolyte and catholyte, respectively, were generated from the stock electrolyte in a large-scale electrolytic flow cell with carbon felt electrodes separated by a Nafion membrane, as previously described.[15]

2.3. Fuel Cell Diagnostics. Polarization data were measured after flow stabilization at a given flow rate by chronoamperometry under stepwise potentiostatic control from 0.0 V to the open circuit voltage, using a PARSTAT 2263 potentiostat (Princeton Applied Research). Increments of 0.2 V were employed for cell polarization, and 0.1 V increments were employed for anode/cathode polarization. The current generated by the cell was monitored until steady state was reached (30−300 s, depending on the flow rate). Anodic and cathodic polarizations were measured using the opposite in-channel carbon electrode as counter electrode and an external saturated calomel reference electrode (SCE) placed in the outlet reservoir. Because of the three-dimensional architecture, the definition of an area with which to characterize the performance of the flow-through cell in terms of current density is somewhat ambiguous. Specifically, the flow-normal area of each electrode is 300 μm × 12 mm (0.036 cm^2), the vertically projected area of each electrode is significantly larger (1 mm × 12 mm = 0.12 cm^2), and the total active surface area within the electrode is estimated as 3 cm^2. Utilization of the high internal surface area is a feature of this fuel cell; however, to make meaningful performance comparison with previous microfluidic fuel cells, current densities and power densities reported here were calculated on the basis of the vertically projected area of the electrodes. It is noteworthy that power-per-volume, while unconventional, is a more pertinent performance metric from a device perspective.

The ohmic resistance of the fuel cell was measured by electrochemical impedance spectroscopy (EIS), using the same potentiostat. Impedance spectra were recorded for each flow rate at the open-circuit cell voltage, by applying an ac amplitude of 5 mV rms over the frequency range from 50 kHz to 0.1 Hz. The combined ohmic cell resistance was obtained from the high-frequency real axis intercept of the Nyquist plot of impedance.

3. Results and Discussion

Microfluidic vanadium redox fuel cell operation is based on the following anodic and cathodic redox reactions and associated standard electrode potentials at 298 K:[19]

$$V^{3+} + e^- \rightleftarrows V^{2+} \qquad E^\circ = -0.496 \text{ V vs SCE} \qquad (1)$$

$$VO_2^+ + 2H^+ + e^- \rightleftarrows VO^{2+} + H_2O \qquad E^\circ = 0.750 \text{ V vs SCE} \qquad (2)$$

The overall cell reaction has a theoretical standard cell potential of 1.246 V. The cell potential can, however, be increased beyond 1.50 V by the use of high-purity vanadium solutions.[9,15] The theoretical maximum current density of a microfluidic fuel cell is controlled by the rate of convective/diffusive transport of reactants and products in the liquid phase to and from the surface of the electrodes. In the limiting case, the concentration of reactant is zero at the surface, and a concentration boundary layer is formed in the channel that limits the flux of reactant to the surface depending on the flow characteristics. Overall fuel cell performance, usually measured by power density, is, however, influenced by other factors as well. In our previous study of microfluidic vanadium redox fuel cells with planar electrodes based on graphite rods,[14] it was found that the performance of the cell was controlled by a combination of species transport, electrochemical kinetics, and ohmic resistance. Improved performance was enabled by the implementation of porous electrodes;[15] the overall electrochemical kinetics was improved by the increased active surface area, and the rate of species transport to the active sites was enhanced by a partial flow velocity inside the top portion of the porous medium, although the penetration depth was limited.

The microfluidic vanadium redox fuel cells employed here are shown schematically in Figure 1. Figure 1c,d provides a schematic comparison of the new flow-through architecture (c) to the established flow-over architecture (d). In contrast to the flow-over cell, the flow-through cell is designed to direct the flow of vanadium fuel and oxidant solutions uniformly through the porous electrode structures. This strategy achieves utilization of the full depth of the electrode and associated active area and provides enhanced species transport from the bulk to the active sites. The electrolyte streams enter the fuel cell on each side via a deep (300 μm) feed section that distributes the flow toward the side of the porous strip electrode (Figure 1b). The flow is guided at a low mean velocity from the feed section orthogonally through the 300 μm-deep and 1 mm-wide porous electrode into the less deep (150 μm) co-laminar exit section, where it is brought downstream to the outlet at a significantly higher mean velocity. The co-laminar exit section, which effectively employs the waste solutions as an ionic charge-transfer medium, was given a high aspect ratio (width/depth) cross-sectional profile to confine the interdiffusion/crossover zone to the center of the channel. In the flow-over cell (Figure 1d), diffusive mixing in the co-laminar channel represents loss of reactant, or fuel/oxidant crossover. In contrast, in the flow-through cell (Figure 1c), the reactants are consumed before reaching the central channel, and the co-laminar streaming merely separates the waste products of the electrodes while providing proton transport. With respect to flow distribution in the flow-through cell, the pressure drop over the porous electrode is estimated to be 2 orders of magnitude higher than the serially connected distribution channel. Assuming an effectively uniform pore distribution, a spatially uniform flow rate of reactant through the porous electrode is expected.

The microfluidic fuel cell prototype with flow-through porous electrodes was operated at flow rates spanning more than 2

(19) *CRC Handbook of Chemistry and Physics*, 83rd ed.; CRC Press: Boca Raton, FL, 2002.

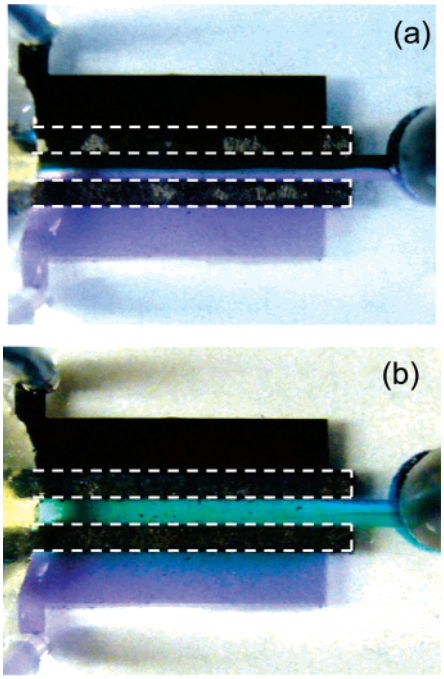

Figure 2. Images obtained during steady-state operation of the microfluidic fuel cell with flow-through porous electrodes at (a) open-circuit and (b) 0.8 V cell voltage. The vanadium electrolytes contain V^{2+} (purple) and V^{3+} (light green) at the anode, and VO_2^+ (black) and VO^{2+} (turquoise) at the cathode. The flow rate was 1 μL min^{-1} per stream. Dashed lines indicate the extent of the porous electrodes.

orders of magnitude, from 1 to 300 μL min^{-1} per stream, using 2 M vanadium ions in 4 M sulfuric acid electrolyte. An advantage inherent to the use of the optically transparent PDMS material in combination with the distinctive colors of the vanadium species is that fuel cell operation under co-laminar flow can be observed visually. Figure 2a shows an image of the fuel cell operating at open-circuit (i.e., no current was drawn from the cell). The anolyte (V^{2+} - violet) and catholyte (VO_2^+ - black) streams passed through the electrodes orthogonally and filled the co-laminar exit section between the electrodes from both sides. The microfluidic co-laminar flow characteristics were maintained toward the outlet, and diffusive mixing was restricted to the center of the channel. The absence of electrochemical reactions at the open-circuit voltage was confirmed by the uniform colors. The image in Figure 2b corresponds to steady-state operation at 0.8 V cell voltage. As current was drawn from the cell, distinctive colors in the co-laminar anolyte and catholyte waste stream were no longer visible. Instead, the waste stream appeared a light green/turquoise characteristic of (V^{3+})/(VO^{2+}) solutions. The distinct change in the waste stream content between Figure 2a,b provided an optical indication that much of the initial vanadium species had undergone electrochemical reaction in the operating cell.

3.1. Polarization and Power Density. Steady-state polarization data were obtained at room temperature under potentiostatic control. The results were also reproducible under galvanostatic control, and the average standard deviation of repeated experimental trials was less than 1% with the same cell and within 7% using different cells. The polarization curves in Figure 3a show steady-state operation of the fuel cell prototype at four different flow rates from 1 to 300 μL min^{-1}. These flow rates correspond to laminar flow characteristic of low Reynolds

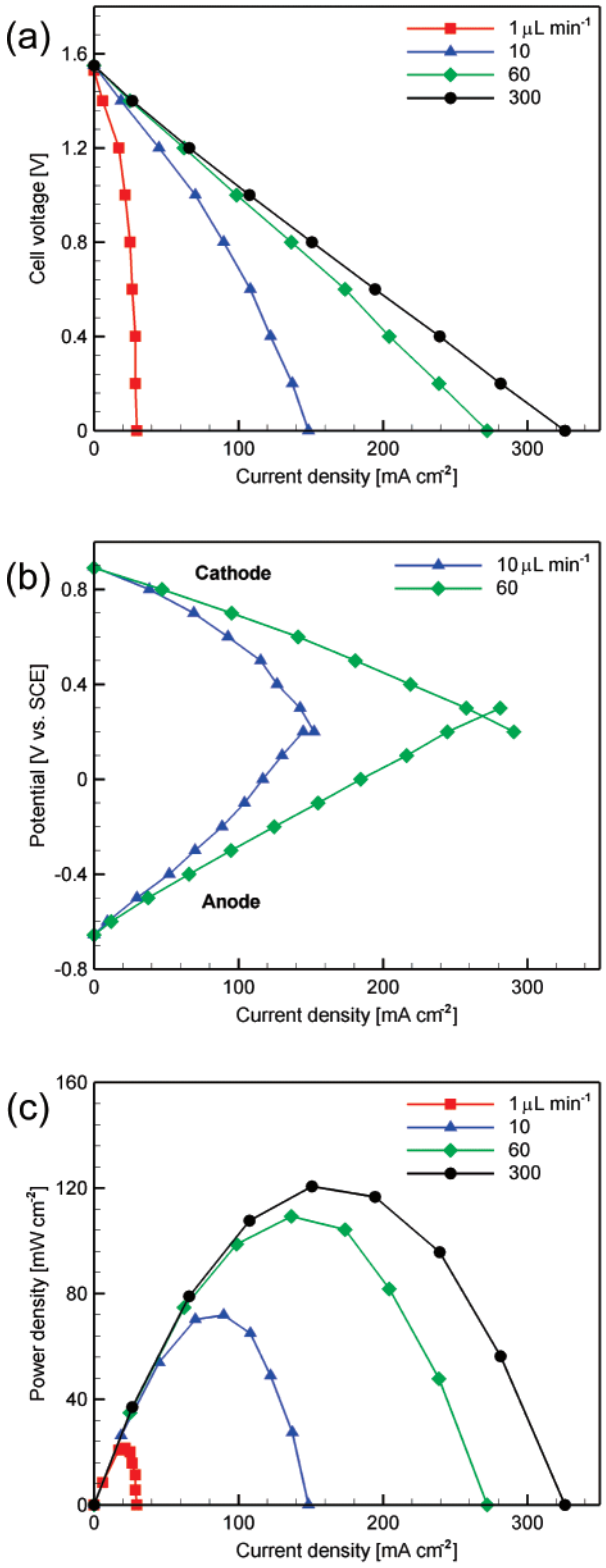

Figure 3. Flow-through fuel cell performance data. (a) Polarization data obtained under potentiostatic control at steady state and room temperature. (b) Steady-state anodic and cathodic polarization data for the flow-through fuel cell measured in situ at room temperature under potentiostatic control, at two different flow rates, using the opposite fuel cell electrode as counter electrode and an external SCE reference electrode. (c) Power density curves obtained from room-temperature fuel cell polarization data. Corresponding flow rates are labeled in each plot.

number, *Re* (*Re* = *UD*/ν, where *U* is the average fluid velocity, *D* is the hydraulic diameter, and ν is the kinematic viscosity).

The highest flow rate used here corresponds to Reynolds numbers from $Re \approx 10^{-2}$ in the porous medium up to $Re \approx 20$ at the outlet of the co-laminar exit channel. The open-circuit voltage of the fuel cell was 1.53−1.55 V, and current densities up to 326 mA cm^{-2} were generated. Several trends can be identified on the basis of these data: As expected, the current density increased with flow rate, which is a consequence of mass transport combined with relatively fast electrochemical redox reactions. However, the steep negative slope observed at the lowest flow rate, associated with predominant mass transport control, becomes less significant as the flow rate is increased. Above 60 μL min^{-1}, the polarization curves become more linear and further increasing the flow rate results in only marginally increased performance. This effect is attributed to the parasitic ohmic voltage loss caused by series resistance in the cell, which is proportional to the current density. The combined ohmic resistance, including both in-channel ionic resistance and electrical resistance in electrodes, contacts, and wires, was measured by EIS to be 27.6 Ω at 300 μL min^{-1}. This value is higher than that for previous cells[9,15] and constitutes 70% of the average slope of the corresponding polarization curve (39.6 Ω).

Individual anodic and cathodic polarization curves obtained versus an external SCE reference electrode are presented in Figure 3b for two different flow rates. This type of plot is normally used in fuel cell analysis to assess which one of the electrodes is limiting the overall fuel cell performance. In this case, a highly symmetric polarization pattern was observed, indicating that neither electrode imposed a dominating restriction on the cell and that the electrochemical system was well-balanced with respect to both electrochemical kinetics and mass transport. This desired characteristic confirms the viability of the proposed flow-through porous electrode architecture for microfluidic fuel cells.

Power density curves, calculated from the polarization data in Figure 3a, are shown in Figure 3c. These results demonstrate high levels of power density, which will be compared with other designs in section 3.2. The overall power density increases considerably with flow rate, which again confirms the partial mass transport control. The highest power density obtained here was 121 mW cm^{-2} at 0.8 V and 300 μL min^{-1}. Operation at higher flow rates would be possible, but with limited gain due to the high ohmic resistance. The parasitic power loss associated with pumping the solutions through the porous electrodes was estimated from the pressure drop for flow within porous media. Specifically, Darcy's Law relating pressure drop to flow parameters was employed assuming a permeability of 10^{-12} m^2 characteristic of the carbon paper. Because of the low Reynolds number of the cross-flow ($Re \approx 10^{-2}$), this pressure drop is quite small. The total pumping power required to sustain the flow through the porous electrodes and the surrounding channel structure[14] is therefore estimated to be less than 1% of the fuel cell output power under typical conditions.

The stability of the current generated by the fuel cell was evaluated by an extended potentiostatic experiment performed at a practical cell voltage (0.8 V) in the low flow rate regime (1 μL min^{-1}), the result of which is shown in Figure 4. After a brief transient period, the current density was quite steady throughout the entire 10 h time period, showing typical variations of ±2%. No performance degradation was detected during this test; in fact, the highest hourly averaged current density in the steady phase was recorded during the eighth hour. Deviations about the average current density are attributed to the low flow rate and the associated unsteady reactant feed; at higher flow rates, the current density is expected to have less noise. Although the exact cause is not known, the comparatively large asperity at 2.6 h could, for instance, have been caused by a small gas bubble in the feed line temporarily interrupting flow of reactant.

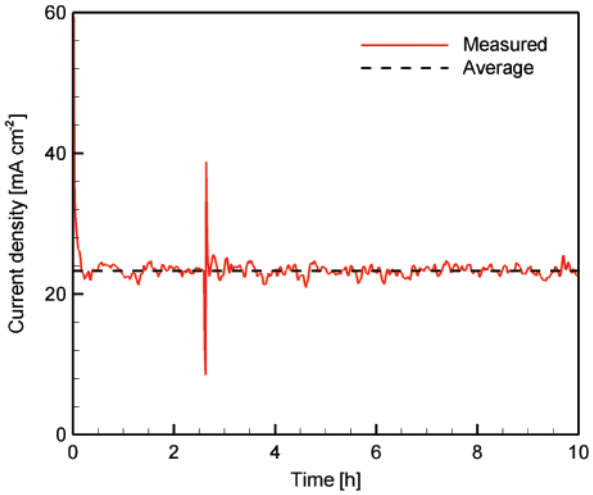

Figure 4. Flow-through fuel cell steady-state chronoamperometric data measured at 0.8 V cell voltage and 1 μL min^{-1} flow rate.

3.2. Performance Comparison. The performance of the microfluidic fuel cell with flow-through porous electrodes is compared to previous results obtained using flow-over architecture cells with planar[14] and untreated porous[15] electrodes mounted on the bottom of the co-laminar flow channel. Also, to evaluate the performance benefits associated with hydrophilic heat-treated porous electrodes, a flow-over cell incorporating hydrophilic porous electrodes was fabricated. In Figure 5, a performance comparison based on (a) peak power density and (b) active fuel utilization at 0.8 V is provided. All plots are given as a function of flow rate per stream, which can be considered a measure of operational cost in terms of reactant supply. Compared to the previously reported flow-over cells using untreated porous electrodes, the flow-through architecture produced notably high power densities across all flow rates tested: the level of improvement ranges from two times at 300 μL min^{-1} to four times at 1 μL min^{-1}. These power density levels confirm that a larger portion of the total active area was being utilized and that the convective/diffusive species transport to the active sites has been improved considerably. The flow-over fuel cell with hydrophilic porous electrodes also generated higher power density than the previous fuel cell with untreated porous electrodes, but generally less than the flow-through architecture. At the highest flow rate, however, the flow-over cell produced the highest peak power density, 131 mW cm^{-2}, as compared to 120 mW cm^{-2} provided by the flow-through cell. The slope of the peak power density curve for the flow-through cell shows diminishing returns at high flow rates. This limitation of the flow-through cell is attributed to the ohmic resistance (28 Ω) that is significantly higher than the flow-over cell (20 Ω), as measured by EIS at 120 μL min^{-1}. Overall, these results highlight the importance of the hydrophilic porous electrode treatment, the effectiveness of the flow-through

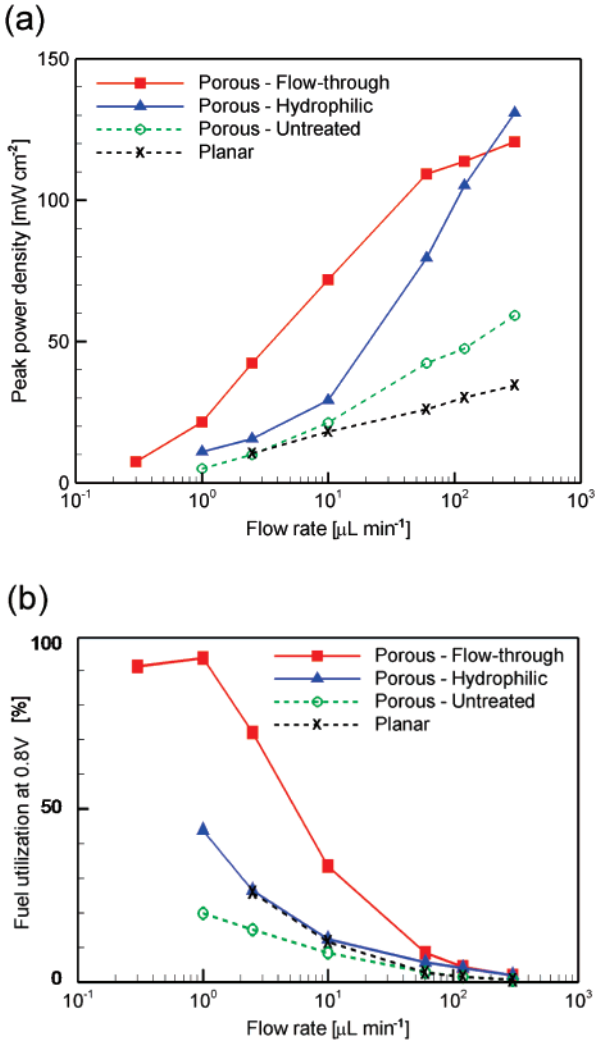

Figure 5. Performance comparison between the flow-through fuel cell and flow-over fuel cells (with electrodes mounted on the bottom of the co-laminar flow channel), in terms of (a) peak power density and (b) active fuel utilization at 0.8 V cell voltage, as a function of the flow rate (logarithmic). The vanadium redox concentrations were 2 M in all cases. The solid lines correspond to the fuel cells developed in this work, whereas the dashed lines correspond to a previously reported flow-over porous electrode fuel cell[15] and a planar microfluidic fuel cell.[14]

architecture, and the potential for significantly increased performance by reducing the ohmic resistance in the flow-through cell.

In addition to high power density levels, high Coulombic fuel utilization per single pass is desirable. Figure 5b presents active fuel utilization measured at a practical cell voltage of 0.8 V as a function of flow rate for the four fuel cell designs under study. The Coulombic fuel utilization was calculated as the current output (converted to flux units) divided by the flux of reactant entering the channel.[14] The flow-through architecture provided higher fuel utilization than all the other designs. The highest fuel utilization measured at this cell voltage was 94%, obtained with the flow-through architecture at 1 μL min^{-1}. At such high levels of fuel utilization, fuel and oxidant crossover is irrelevant, given that essentially all the reactants have been consumed while passing through the electrodes. The ability to combine high fuel utilization with high power density at high operational cell voltage is unique to the flow-through microfluidic fuel cell

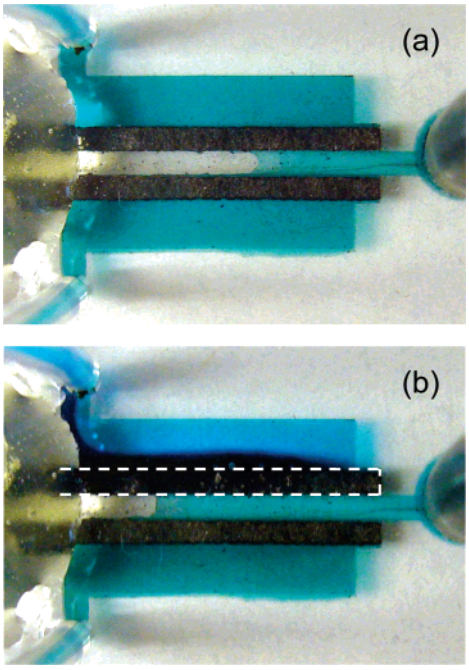

Figure 6. Images demonstrating the in situ regeneration capability of the new microfluidic fuel cell architecture when operated on the all-vanadium redox system. Fully mixed waste solution (~50/50 V^{3+}/VO^{2+}) is flowing in the reverse direction from right to left at 1 μL min^{-1} per stream, and a cell voltage of (a) 0.0 V (open-circuit) and (b) 1.5 V is applied to the cell. Dashed lines indicate the extent of the porous electrodes.

architecture presented here. At 0.8 V, for example, the fuel cell produced 20 mW cm^{-2} combined with 94% active fuel utilization under steady-state operation. On the basis of the theoretical standard cell potential (1.246 V), this is equal to an overall single pass energy conversion efficiency of 60%.

If the reactions described in eqs 1 and 2 are completed for all respective species, the fuel utilization is considered 100%. It is noteworthy, however, that the produced species still constitute a redox pair (i.e., V^{3+}/VO^{2+}), and thus there is potential to gain further electrons from their reaction at the respective electrodes. Through this effect, nominal fuel utilization over 100% was in fact obtained at low flow rates and low operational cell voltages ($\leq$0.4 V). The data presented in Figure 5b were measured at a more practical cell voltage of 0.8 V, where the current contribution from the secondary redox reaction is negligible.

3.3. In Situ Regeneration. With the flow-through microfluidic fuel cell architecture demonstrated here, there is the additional opportunity for in situ regeneration. The initial fuel and oxidant species can be regenerated by running the cell in an electrolytic format (i.e., pumping waste solution back into the cell and applying an electrolytic cell voltage). Figure 6 shows images obtained during reverse operation. Although an air bubble was present in the central channel, it was possible to establish proof-of-concept regeneration with this cell. While holding the cell potential at 0.0 V and running the reverse flow at 1 μL min^{-1}, the cell current was zero and the solutions were green in both half cells (Figure 6a). Thereafter, the applied cell potential was held constant at 1.5 V while running the cell in reverse for 30 min (Figure 6b). In this case, purple V^{2+} and black VO_2^+ were identified in the anodic and cathodic half cells, respectively, and a steady regeneration current with a time-averaged current density of 45 mA cm^{-2} was measured.

Eventual integration of a regenerative flow-through fuel cell device will require development of supporting infrastructure beyond the scope of this work. It is possible, however, to consider liquid volume requirements. With a run time of 6 h at 10 μL/min per inlet stream (producing $\sim$70 mW cm^{-2}, or 8.4 mW) the cell would require 3.6 mL of fuel, 3.6 mL of oxidant, and thus a waste liquid volume capacity of 7.2 mL. Our current focus is to study the operation in the regenerative mode and investigate the feasibility and roundtrip efficiency of a regenerative microfluidic fuel cell (i.e., a microfluidic battery), based on the fuel cell architecture demonstrated here.

4. Conclusions

In this work, a microfluidic fuel cell architecture incorporating flow-through porous electrodes and employing the all-vanadium redox system was presented. In contrast to previous work, the flow-through architecture is designed to direct the flow of fuel and oxidant solutions uniformly through the porous electrode structures before combination of the waste streams in a co-laminar format. This strategy achieves utilization of the full depth of the porous electrode and associated active area and provides enhanced species transport from the bulk to the active sites. Performance levels that are unprecedented to date for microfluidic fuel cells were demonstrated: power densities up to 131 mW cm^{-2}, near complete fuel utilization, and high operational cell voltages. The fuel cell also had the capability to combine these three characteristics during steady-state operation, resulting in high overall energy conversion efficiency. We expect performance would further benefit from increasing the concentration of the vanadium redox species, optimizing the microstructure and porosity of the flow-through carbon electrodes, and most importantly, reducing the combined ohmic resistance of the cell. In addition, proof-of-concept in situ regeneration of the initial fuel and oxidant species was established by running the fuel cell in reverse.

Acknowledgment. This research was funded by the Natural Sciences and Engineering Research Council of Canada (NSERC) and Angstrom Power, Inc. Experimental assistance provided by Dr. Clive Brereton and Evan Hobenshield at NORAM Engineering and Constructors Ltd. and infrastructure funding from Canada Foundation for Innovation (CFI) were highly appreciated.

JA078248C